Hydrazine Oxidation in Aqueous Solutions I. N4H4 Decomposition

Martin Breza * and Anton Gatial

Posted Date: 1 July 2024

doi: 10.20944/preprints202407.0102.v1

Keywords: Coupled Cluster; geometry optimization; N-N bond fission; QTAIM analysis; electron structure

Article

Hydrazine oxidation in aqueous solutions II. N_4H_4 decomposition

Martin Breza [1,*] and Anton Gatial [2]

[1] Dept. Physical Chemistry, Slovak Technical University, Radlinskeho 9, SK-81237 Bratislava, Slovakia; martin.breza@stuba.sk
[2] Dept. Physical Chemistry, Slovak Technical University, Radlinskeho 9, SK-81237 Bratislava, Slovakia; anton.gatial@stuba.sk
* Correspondence: martin.breza@stuba.sk

Abstract: Oxidation of a mixture of nonlabelled ($^{14}N_2H_4$) and ^{15}N labeled ($^{15}N_2H_4$) hydrazine in aqueous solutions produces $^{14}N^{15}N$ molecules, indicating the intermediate existence of N_4H_6 or N_4H_4 dimers with subsequent transfers of H atoms and splitting of lateral N-N bonds. To explain the key part of hydrazine oxidation reaction, the structures, thermodynamics, and electron characteristics of N_4H_4 molecules in aqueous solution are investigated at CCSD/cc-pVTZ level of theory. We have not found any spontaneous splitting of the bond between lateral nitrogen atoms in tetrazenes N_4H_4 during geometry optimization. The most probable N_4H_4 oxidation products are H_2N-NH_2 and N_2, which are obtained by splitting the bond between central nitrogen atoms and so only $^{15}N_2$ and $^{14}N_2$ molecules are formed. Additionally, the formation of H_3N-NH and N_2 oxidation products is also preferred to structures without any N-N fissions. The formation of H_2N=N and HN=NH reaction products is energetically less advantageous. Cyclo-N_4H_4 structures are stable, without any N-N fissions, but their very high Gibbs energies indicate their vanishing abundance in aqueous solution, so their involvement in hydrazine oxidation is highly improbable. Hydrazine oxidation to $^{14}N^{15}N$ molecules cannot be explained by tetrazene N_4H_4 intermediates.

Keywords: Coupled Cluster; geometry optimization; N-N bond fission; QTAIM analysis; electron structure

1. Introduction

Hydrazine N_2H_4 is used as a rocket propellant, antioxidant, a pesticide precursor, a corrosion inhibitor in boilers, etc. [1,2]. However, hydrazine is toxic and its exposure can injure the lungs, liver, kidney, and central nervous system of living organisms [3]. Therefore, the study of the exact mechanism ofhydrazine oxidation is of permanent interest.

The stoichiometry of the decomposition of hydrazine depends on the relative concentrations of OH^-, c(OH-) and hydrazine, $c(N_2H_4)$ [4,5].

$$(6 + x)\ N_2H_4 \rightarrow (x + 2)\ N_2 + 8\ NH_3 + 2x\ H_2 \quad (1)$$

where $x = c(OH^-)/c(N_2H_4)$. For $x >> 1$ is $dc(NH_3)/dt \rightarrow 0$ and for $x << 1$ is $dc(H_2)/dt \rightarrow 0$. Depending on the reaction conditions, different stiochiometry is also possible [6].

Mass spectroscopic analysis of nitrogen molecules obtained by oxidation of ^{15}N-enriched hydrazine by various oxidizing agents in aqueous solutions produced $^{14}N_2$, $^{15}N^{14}N$ and $^{15}N_2$ molecules [7,8]. The relative content of the $^{15}N_2$ and $^{15}N^{14}N$ molecules depends on the oxidizing agent used. Thus, some of nitrogen molecules must be formed by a mechanism including a N-N fission and the formation of the nitrogen-containing radicals from two different hydrazine molecules.

$$^{15}NH_2\text{-}^{15}NH_2 + {}^{14}NH_2\text{-}^{14}NH_2 \rightarrow {}^{15}NH_2\text{-}^{15}NH\bullet + \bullet{}^{14}NH\text{-}^{14}NH_2 \rightarrow {}^{15}NH_2\text{-}^{15}NH\text{-}^{14}NH\text{-}^{14}NH_2 \quad (2)$$

$$^{15}NH_2\text{-}^{15}NH\text{-}^{14}NH\text{-}^{14}NH_2 \rightarrow \quad \cdots \quad \rightarrow \quad {}^{15}NH_3 + {}^{15}N^{14}N + {}^{14}NH_3 \quad (3)$$

 doi:10.20944/preprints202407.0102.v1

According to Cahn and Powell [8] the randomized $^{15}N^{14}N$ composition is obtained by one-electron oxidation of ^{15}N enriched hydrazines whereas four-electron oxidizing agents (acid iodate, alkaline ferricyanide) produce unrandomized N_2 molecules (all four hydrogen atoms are removed from a single hydrazine molecule). According to Petek and Bruckenstein [6] the electrooxidation of ^{15}N labeled hydrazine (96.7% enrichment) on the Pt electrode produces N_2 molecules with the ratio of $^{14}N^{15}N/^{15}N^{15}N = 0.07 \pm 0.01$ while in Ce(IV) solutions it was 0.9 ± 0.2. Simultaneous electrooxidation and homogeneous oxidation with electrogenerated Ce(IV) produced both isotopic forms between these two limits.

Cahn and Powell [8] mentioned an alternative way of oxidation of hydrazine through diimine HN=NH intermediate as well.

$$2\ HN{=}NH \rightarrow \quad HN{=}N{-}NH{-}NH_2 \quad \rightarrow \quad HN_3 + NH_3 \tag{4}$$

Polarographic and voltammetric studies of hydrazine in solutions of intermediate acidity (e.g., 0.025 – 0.25 M H_2SO_4) indicate that higher initial hydrazine concentrations cause proportionally increased concentrations of diimine N_2H_2 and therefore its dimerization rate to tetrazene N_4H_4 increases more rapidly than the rate of further oxidation according to the Equation (4) [9]. Other authors [10,11] mentioned an alternative disproportionation mechanism as well.

$$2\ HN{=}NH \rightarrow \quad H_2N{-}N{=}N{-}NH_2 \quad \rightarrow \quad N_2 + H_2N{-}NH_2 \tag{5}$$

The relative stability of 2-tetrazene $H_2N{-}N{=}N{-}NH_2$ in trans-conformation is confirmed by its X-ray structure determined at -90 °C [12].

The randomized $^{15}N^{14}N$ composition in the case of high concentrations of tetrazene N4H4 can be explained in analogy with Equations (2) and (3) as follows

$$^{15}NH{-}^{15}NH + {}^{14}NH{-}^{14}NH \rightarrow {}^{15}NH{-}^{15}NH{-}^{14}NH{-}^{14}NH \rightarrow {}^{15}NH_2{-}^{15}N{=}^{14}N{-}^{14}NH_2 \tag{6}$$

$$^{15}NH_2{-}^{15}N{=}^{14}N{-}^{14}NH_2 \rightarrow \bullet{}^{15}NH_2 + {}^{15}N^{14}N + \bullet{}^{14}NH_2 \tag{7}$$

$$\bullet{}^{15}NH_2 + \bullet{}^{14}NH_2 \rightarrow {}^{15}NH_2{-}^{14}NH_2 \tag{8}$$

Quantum-chemical studies of tetrazenes are very rare. Zhao and Gimarc [13] investigated the strain energies of $(NH)_n$ rings, n = 3 – 8, at the Hartree-Fock and MP2 levels of theory using the 6-31G** basis sets. They found the maximal ring strain for n = 4. The preferred ring conformations have nearly perpendicular lone electron pairs on adjacent N atoms (the gauche effect). Ball [14] evaluated the vibrational heats of formation of four stereoisomers of cyclo-$(NH)_4$ at several post-Hartree-Fock theoretical levels. Feng et al. [15] studied the structures, charges, isomerization and decomposition of four tripodal (unusable for our purposes) and ten linear (*anti*-conformation) N_4H_4 structures at the CCSD(T)/cc-pVTZ level of theory using B3LYP/6-311++G(d,p) optimized geometries. Hu and Zhang [16] performed periodic DFT molecular dynamics calculations of high-pressure N_4H_4 structures at zero temperature. In the pressure range 30 – 100 GPa, three stable $P2_1/m$ structures were found, namely the $(NH)_4$ solid in trans-conformation and an ambient pressure *trans*-2-tetrazene $H_2N{-}N{=}N{-}NH_2$ and the most stable ammonium azide. Two additional molecular N_4H_4 structures ($H_2N{-}N{-}NH{-}NH$ in *trans*-conformation and $NH_3 \ldots HN_3$) and three transition states were also found.

In our previous study [17] we have investigated the structures, thermodynamics, and electron characteristics of various N_4H_6 isomers in aqueous solutions by means of quantum chemistry at the CCSD/cc-pVTZ level of theory. The aim of our previous study was to explain the existence of $^{14}N^{15}N$ molecules obtained by the homogenous oxidation of a mixture of non-labeled ($^{14}N_2H_4$) and ^{15}N-labeled hydrazine ($^{15}N_2H_4$) in an aqueous solution according to the Equations (1)–(3). We focused on the N – N fissions in N_4H_6 structures obtained by hydrogen rearrangements as a crucial part of the entire oxidation reaction. The dominant abundance of $NH_3 \ldots N_2 \ldots NH_3$ species according to Gibbs energies obtained by splitting the lateral N – N bonds is in full agreement with the $^{14}N^{15}N$ molecules formation. Except for stable cyclo-$(NH)_4$. H_2 structure, the initial cyclic structures are split into hydrazine and N_2H_2 species in agreement with the $^{14}N^{15}N$ molecules formation but their abundance in aqueous solutions is vanishing.

 doi:10.20944/preprints202407.0102.v1

Above, we have shown that the oxidation of hydrazine in solutions of intermediate acidity into $^{15}N^{14}N$ molecules can proceed through N_4H_4 intermediates according to Equations (6)–(8) as well [9–11]. In analogy to [17], the main aim of our manuscript is a quantum-chemical study of N_4H_4 isomers in aqueous solutions and to determine the sites of possible N – N fissions in these molecules. The Gibbs energies of the decomposed N_4H_4 products allow us to predict the formation of $^{14}N^{15}N$ in real systems. Thus we are interested dominantly in the nitrogen backbone and its possible fissions. The electronic structures of the stable isomers will be compared as well.

2. Results

In analogy to our previous study [17], we use the linear backbone notation N1-N2-N3-N4 and the composition notation of $N1H_m$-$N2H_n$-$N3H_p$-$N4H_q$, where subscripts m, n, p and q denote the number of H atoms bonded to individual Nj atoms with j = 1 → 4 and m + n + p + q = 4. Geometry optimizations started with planar *anti*- and *syn*-conformations of the N1-N2-N3-N4 backbone denoted Amnpq and Bmnpq, respectively. During geometry optimization some N - H bonds can be split and the new ones can be created. In such cases, the original notation is preserved only with new values of m, n, p, or q. Alternatively, some N – N bonds can split and new structures with destroyed N1-N2-N3-N4 backbones are denoted as D(mn)(pq) or D(m)(npq), where the individual components are enclosed in round brackets. If new N – N bonds are formed instead of the split ones, the obtained structures are denoted with the letter E such as Emn)(pq. This means that the N2 – N3 bond is split and a new N1 – N4 bond is created, i.e., the new composition $N2H_n$-$N1H_m$-$N4H_q$-$N3H_p$. In general, if N1 and N2 atoms are ^{15}N labeled, while N3 and N4 correspond to ^{14}N, then splitting the N1-N2 and N3-N4 bonds would lead to $^{14}N^{15}N$ molecules, unlike N2-N3 fissions.

An analogous notation Cmnpq is used for cyclo-N_4H_4 isomers. In these structures, any N – N fission can lead to the formation of the $^{15}N^{14}N$ molecules as a consequence of suitable H transfers within the cycle.

The different structures with the same Xmnpq notation, X = A, B, C, D or E, are distinguished by additional letters a, b, c, d, etc. at the end of the Xmnpq symbol, such as D(mn)(pq)b. These structures differ in energies because of different hydrogen bonding patterns.

Among the starting structures in *anti*-conformations, A2020 is transformed into A2011 and A4000 into A3010 due to H transfers from N3 to N4 and from N1 to N3 (see Table 1 and Figure 1). Both structures are practically identical to those obtained by geometry optimizations of original A2011 and A3010, respectively. A0220 is split into two $H_2N{=}N$ species, A1210 and A2200 are split into H_2N-NH_2 and N_2, A1120 into HN=NH and H2N = N, while A3100 is split into NH_3-NH and N_2. In general, N2-N3 fissions cannot finally lead to $^{14}N^{15}N$ molecules. According to Gibbs energy data (Table 1), three of these split structures belong to the most stable intermediates of hydrazine oxidation reactions. The remaining anti-conformers preserve their original structures with only small changes (Table 1, Figure 1).

Table 1. N1-N2-N3-N4 dihedral angles (Θ_{1234}), absolute (G_{298}) and relative (ΔG_{298}) Gibbs free energies at 298.15 K of the optimized N_4H_4 structures obtained from the starting ones. The different structures with the same notation are distinguished by additional letters a, b, c, or d. The most stable structure is highlighted in bold.

Starting	Optimized	Θ_{1234} [°]	G_{298} [Hartree]	ΔG_{298} [kJ/mol]	Remarks
A0220	D(02)(20)	-180.0	-220.84657	-251.26	$N{=}NH_2 + H_2N{=}N$
A1210	D(22)(00)a	31.8	-221.02068	-4822.61	H_2N-$NH_2 + N_2$
A1201	A1201	-106.4	-220.84934	-323.99	
A1120	D(11)(20)a	-179.1	-220.87553	-1011.62	$HN{=}NH + H_2N{=}N$
A1111	A1111	180.0	-220.83700	0.00	
A2200	**D(22)(00)b**	**-176.2**	**-221.02115**	**-4834.95**	**H_2N-$NH_2 + N_2$**
A2110	A2110	-152.4	-220.87955	-1117.17	
A2101	A2101	153.9	-220.91446	-2033.75	
A2020	A2011	180.0	-220.89237	-1453.77	3→4 H rearrangement

 doi:10.20944/preprints202407.0102.v1

A2011	A2011	-180.0	-220.89237	-1453.77	
A2002	A2002	173.0	-220.93100	-2468.02	
A3100	D(31)(00)a	176.3	-220.96823	-3445.51	H_3N-NH + N_2
A3010	A3010	-180.0	-220.84234	-140.20	
A3001	A3001	180.0	-220.89414	-1500.24	
A4000	A3010	180.0	-220.84232	-139.87	1→3 H rearrangement
B0220	D(02)(20)	0.0	-220.84657	-251.26	N=NH_2 +H_2N=N
B1210	E12)(10	-9.9	-220.91726	-2107.27	N2-N3 fission, N1-N4 bonding, → B2101
B1201	D(22)(00)c	-2.3	-221.02062	-4821.03	H_2N-NH_2 + N_2
B1120	D(11)(20)b	-180.0	-220.87565	-1014.78	HN=NH + H_2N=N
B1111	B1111	-2.7	-220.84994	-339.75	
B2200	D(22)(00)d	17.8	-221.02057	-4819.72	H_2N-NH_2 + N_2
B2110	B2110	17.9	-220.87548	-1010.31	
B2101	B2101	-18.7	-220.91727	-2107.53	
B2020	B2020	-0.2	-220.74152	2506.88	
B2011	B2011	-2.4	-220.89749	-1588.20	
B2002	B2002	-4.2	-220.93084	-2463.82	
B3100	D(31)(00)b	29.0	-220.96692	-3411.11	H_3N=NH + N_2
B3010	B3010	0.0	-220.85489	-469.71	
B3001	B3001a	0.0	-220.90266	-1723.94	
B4000	B3001b	0.0	-220.89253	-1457.97	1→4 H rearrangement
C1111	C1111	11.8	-220.84534	-218.97	
C2200	C2200	-31.2	-220.71366	3238.35	
C2110	C2110	-18.7	-220.79133	1199.09	
C2101	C2101	27.8	-220.77308	1678.25	
C2020	C2020	0.0	-220.77314	1676.68	

 doi:10.20944/preprints202407.0102.v1

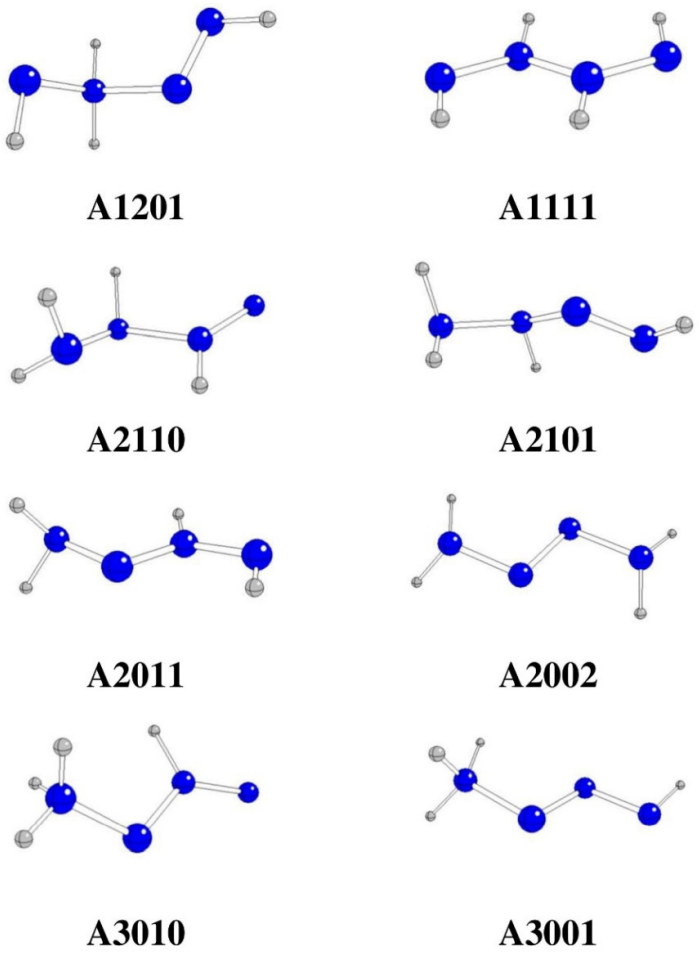

Figure 1. Optimized stable N_4H_4 structures in *anti*-conformation (N – blue, H – gray).

All starting cyclo-N_4H_4 structures preserve their (nearly) original conformations without any H transfers or N-N fissions (Table 1, Figure 3). However, their Gibbs energies are relatively high (in agreement with [13]) and therefore it is highly unlikely (maybe except C1111) that they can serve as intermediates of hydrazine oxidation.

 doi:10.20944/preprints202407.0102.v1

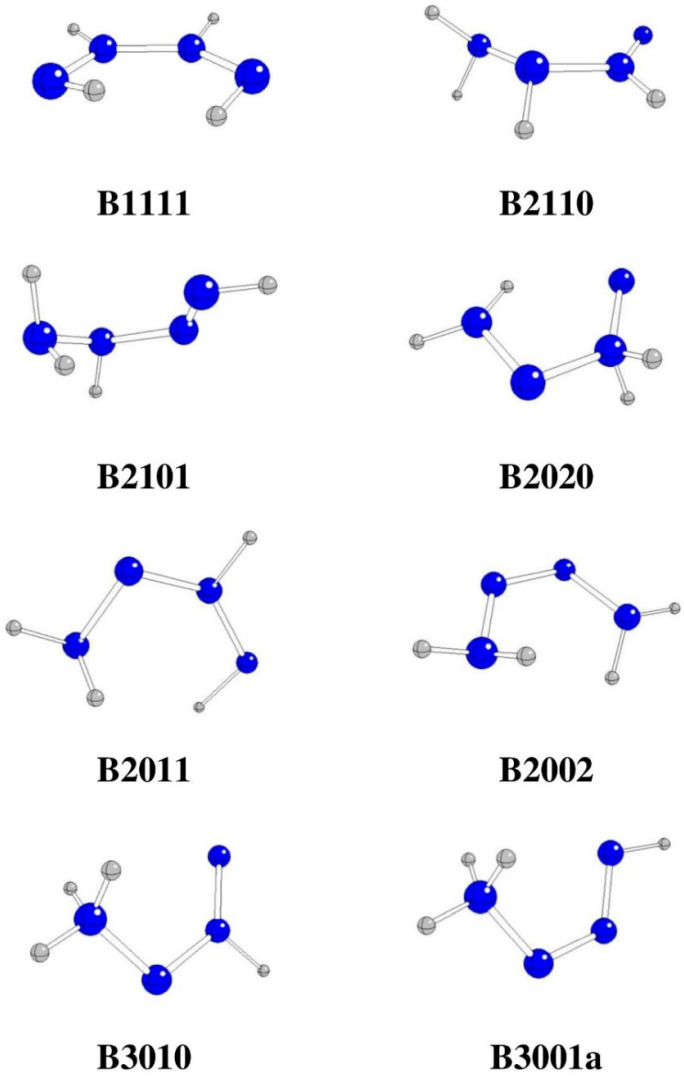

Figure 2. Optimized stable N_4H_4 structures in *syn*-conformation (N – blue, H – gray).

 doi:10.20944/preprints202407.0102.v1

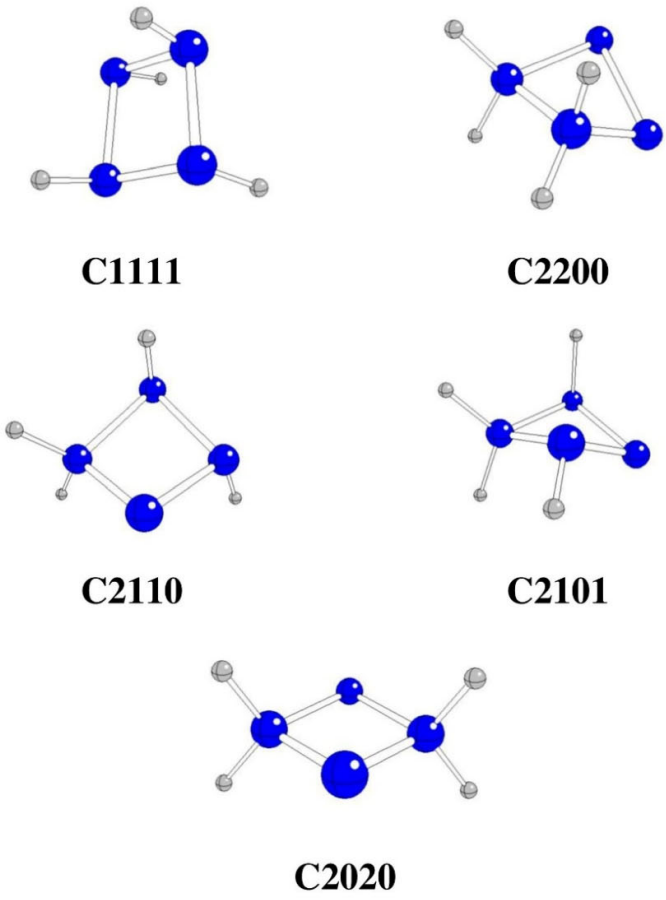

Figure 3. Optimized stable cyclo-N_4H_4 structures (N – blue, H – gray).

The last group of the systems under study is the D(mn)(pq) one. Unlike our previous study of N_4H_6 isomers [17], N_4H_4 isomers are spontaneously split at N2-N3 bonds only. Geometry optimization of possible N_4H_4 isomers indicates that only the $N1H_m$-$N2H_n$ and $N3H_p$-$N4H_q$ subsystems can be obtained by possible hydrogen rearrangements (Table 1, Figure 4).

 doi:10.20944/preprints202407.0102.v1

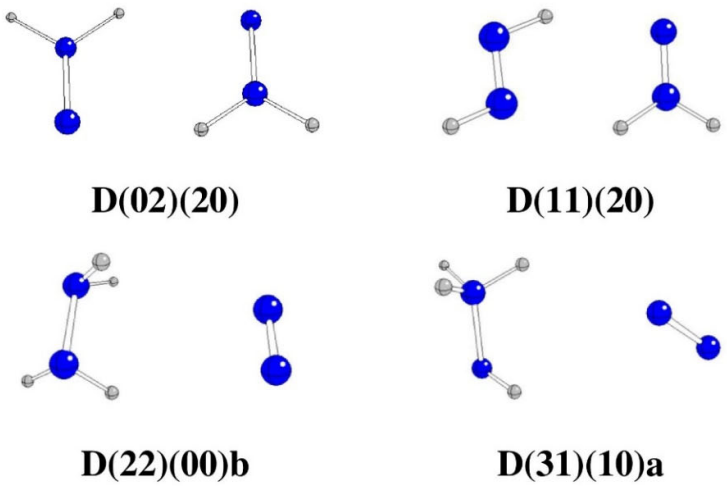

Figure 4. Optimized stable N_4H_4 structures after N – N bond fission (N – blue, H – gray).

The bonding properties of N_4H_4 isomers are described in terms of individual bond lengths (Tables 2 and 3) and in terms of Quantum Theory of Atoms-in-Molecules (QTAIM) [18] such as the electron density ϱ_{BCP} (Tables 4 and 5) and ellipticity ε_{BCP} (Tables 6 and 7) at their bond critical points (BCP). Molecular graphs consist of critical points and bond paths between individual atoms. The bond strengths decrease with bond lengths and increase with their BCP electron densities ϱ_{BCP}. Their double bond character in acyclic structures increases with their BCP ellipticities ε_{BCP}. However, in cyclic structures, increased ε_{BCP} values may reflect mechanical bond strain. According to our previous study of N_4H_6 isomers [17] single, double and triple N-N bonds exhibit BCP electron densities of around 0.2, 0.5 and 0.7 e/Bohr^3, respectively, with BCP ellipticities of ca 0.0, 0.2 and 0.0, respectively. Our results for N_4H_4 isomers are in agreement with these values despite the $N1H_3$-N2 bond lengths in A3010, A3001, B3010 and B3001a-b of ca 1.5 Å indicate weaker bonding. Except for A1201, the BCP ellipticity of the central N1 – N3 bonds is higher than that of the lateral N1 – N2 and N3 – N4 bonds. The significant deviations from N1-N2-N3-N4 planarity (such as in A1201, A2110, A2101, B2110, B2101) in agreement with the gauche effect [14] decrease the BCP ellipticity (i.e. the π character) of N2-N3 bonds. The BCP electron density of N-N bonds decreases with the number of H atoms bonded to these N atoms. In cyclic structures, this dependence is less evident. The characteristics of N-H bonds exhibit high similarities as well. Higher ε_{BCP}(N-H) values can be ascribed mainly to the double-bond character of neighboring N-N bonds, as in [17]. The hydrogen bonds N…H and non-bonding interactions N...N (see Tables 4–7 and Figures S1–S4 in the Supplementary Materials) affect the above bonding properties as well.

The D systems consist of two independent molecules such as HN=NH, H_2N=N, H_2N-NH_2, H_3N-NH or N_2, which mutually interact through weak N…H hydrogen bonds and/or N…N non-bonding interactions only. These molecules were investigated in our previous study on N_4H_6 [17], so their properties are not discussed here in more detail.

 doi:10.20944/preprints202407.0102.v1

Table 2. Interatomic distances (in Å) in the optimized Amnpq and Bmnpq structures. The different structures with the same notation are distinguished by additional letters a or b.

Structure	N1-N2	N2-N3	N3-N4	N1-H	N2-H	N3-H	N4-H
A1201	1.409	1.501	1.225	1.017	1.021(2×)	-	1.025
A1111	1.324	1.288	1.324	1.019	1.015	1.019	1.015
A2110	1.414	1.463	1.190	1.009 1.012	1.016	1.035	-
A2101	1.410	1.370	1.243	1.011 1.014	1.013	-	1.020
A2011	1.437	1.280	1.276	1.015(2×)	-	1.023	1.022
A2002	1.389	1.236	1.389	1.010 1.015	-	-	1.010 1.015
A3010	1.459	1.396	1.210	1.016 1.022(2×)	-	1.040	-
A3001	1.458	1.306	1.278	1.018(2×) 1.022	-	-	1.016
B1111	1.311	1.294	1.311	1.018	1.012	1.012	1.018
B2110	1.405	1.485	1.187	1.009 1.012	1.017	1.031	-
B2101	1.408	1.359	1.246	1.013 1.018	1.007	-	1.019
B2020	1.352	1.433	1.342	1.004 1.025	-	1.026 1.038	-
B2011	1.400	1.276	1.294	1.010 1.021	-	1.014	1.017
B2002	1.388	1.243	1.388	1.009 1.016	-	-	1.009 1.016
B3010	1.437	1.382	1.218	1.015 1.023(2×)	-	1.030	-
B3001a	1.485	1.288	1.286	1.014 1.021(2×)	-	-	1.015
B3001b	1.507	1.289	1.277	1.015 1.021(2×)	-	-	1.025

Table 3. Interatomic distances (in Å) in the optimized Cmnpq and Dmnpq structures. The different structures with the same notation are distinguished by additional letters a, b, c, or d.

Structure	N1-N2	N2-N3	N3-N4	N1-N4	N1-H	N2-H	N3-H	N4-H
C1111	1.469	1.469	1.469	1.469	1.018	1.018	1.018	1.018
C2200	1.434	1.491	1.511	1.495	1.032 1.023	1.032 1.023	-	-
C2110	1.459	1.467	1.488	1.484	1.019 1.024	1.020	1.023	-
C2101	1.457	1.479	1.530	1.456	1.022 1.023	1.023	-	1.020
C2020	1.468	1.468	1.468	1.468	1.019(2×)	-	1.019(2×)	-
D(02)(20)	1.226	3.133	1.226	3.375	-	1.028 1.032	1.028 1.032	-
D(11)(20)a	1.245	3.386	1.224	3.314	1.027	1.029	1.028(2×)	-
D(11)(20)b	1.245	3.064	1.223	3.168	1.029	1.027	1.028(2×)	-
D(22)(00)a	1.445	3.709	1.096	3.492	1.011 1.014	1.011 1.014	-	-

 doi:10.20944/preprints202407.0102.v1

D(22)(00)b	1.445	3.756	1.096	3.893	1.011 1.014	1.011 1.014	-	-
D(22)(00)c	1.445	3.758	1.096	3.461	1.011 1.014	1.011 1.014	-	-
D(22)(00)d	1.445	3.705	1.096	3.706	1.011 1.014	1.011 1.014	-	-
D(31)(00)a	1.466	3.418	1.096	4.353	1.014 1.020(2×)	1.018	-	-
D(31)(00)b	1.466	3.545	1.096	3.742	1.014 1.020(2×)	1.018	-	-

Table 4. BCP electron density (in e/Bohr3) of N-N and N-H bonds in the optimized Amnpq and Bmnpq structures. The different structures with the same notation are distinguished by additional letters a or b. Data for additional N…H hydrogen bonds are presented in parentheses.

Structure	N1-N2	N2-N3	N3-N4	N1-H	N2-H	N3-H	N4-H
A1201	0.3088	0.5150	0.3426	0.3426	0.3505(2×)	-	0.3441
A1111	0.3805	0.4345	0.3805	0.3415	0.3491	0.3491	0.3415
A2110	0.3203	0.2944	0.5366	0.3535 0.3503	0.3504	0.3350	-
A2101	0.3233	0.3662	0.4891	0.3525 0.3495	0.3506	-	0.3494
A2011	0.3054	0.4439	0.4393	0.3489(2×)	-	0.3461	0.3428
A2002	0.3442	0.5015	0.3442	0.3514 0.3462	-	-	0.3514 0.3462
A3010	0.2815	0.3389	0.5083	0.3478 0.3442(2×)	-	0.3325	-
A3001	0.2866	0.4237	0.4459	0.3447(2×) 0.3421	-	-	0.3504
B1111	0.3959	0.4279	0.3959	0.3429	0.3506	0.3506	0.3429
B2110	0.3267	0.2784	0.5386	0.3530 0.3505	0.3497	0.3388	-
B2101	0.3236	0.3726	0.4848	0.3511 0.3456	0.3564	-	0.3498
B2020	0.3717	0.3104	0.3743	0.3536 0.3307	-	0.3359 0.3168	(0.0466)
B2011	0.3338	0.4460	0.4172	0.3524 0.3401	-	0.3548	0.3469
B2002	0.3435	0.4883	0.3435	0.3531 0.3435	-	-	0.3531 0.3435
B3010	0.2990	0.3503	0.4972	0.3496 0.3430(2×)	-	0.3424	-
B3001a	0.2670	0.4397	0.4356	0.3504 0.3432(2×)	-	-	0.3506
B3001b	0.2517	0.4336	0.4395	0.3484 0.3422(2×)	-	-	0.3395

 doi:10.20944/preprints202407.0102.v1

Table 5. BCP electron density (in e/Bohr3) of N-N and N-H bonds in the optimized Cmnpq and Dmnpq structures. The different structures with the same notation are distinguished by additional letters a, b, c, or d. Data for additional N…H hydrogen bonds are presented in parentheses.

Structure	N1-N2	N2-N3	N3-N4	N1-N4	N1-H	N2-H	N3-H	N4-H
C1111	0.2916	0.2916	0.2916	0.2916	1.018	1.018	1.018	1.018
C2200	0.3175	0.2566	0.2620	0.2542	0.3384 0.3450	0.3383 0.3451	-	-
C2110	0.2964	0.2917	0.2759	0.2665	0.3498 0.3467	0.3522	0.3496	-
C2101	0.2940	0.2946	0.2470	0.2785	0.3465 0.3464	0.3513	-	0.3522
C2020	0.2815	0.2808	0.2819	0.2817	0.3530 0.3532	-	0.3536(2×)	-
D(02)(20)a	0.4964	-	04964	-	(0.0233)	0.3422 0.3383	0.3422 0.3383	(0.0233)
D(11)(20)a	0.4863	-	0.4986	-	0.3484 (0.0158)	0.3471	0.3426(2×)	(0.0194)
D(11)(20)b	0.4864	-	0.4986	-	0.3471	0.3484 (0.0157)	0.3426(2×)	(0.0193)
D(22)(00)a	0.2955	-	0.7139	0.0036	0.3530 0.3500	0.3530 0.3503	(0.0027)	-
D(22)(00)b	0.2957	-[(a)]	0.7138	-	0.3530 0.3502	0.3530 0.3500	(0.0038)	(0.0027)
D(22)(00)c	0.2957	-	0.7139	0.0039	0.3530 0.3503	0.3530 0.3500	(0.0026)	-
D(22)(00)d	0.2958	0.0023	0.7140	-	0.3530 0.3503	0.3531 0.3503	-	(0.0027)
D(31)(00)a	0.2685	0.0048	0.7139	-	0.3525 0.3491 0.3486	0.3408	(0.0057)	-
D(31)(00)b	0.2681	-	0.7139	-	0.3525 0.3492 0.3483	0.3412	(0.0043)	(0.0024)

Remarks: [(a)] BCP electron density of the N1-N3 bond is 0.0038 e/Bohr3.

Table 6. BCP ellipticity of N-N and N-H bonds in the optimized Amnpq and Dmnpq structures. The different structures with the same notation are distinguished by additional letters a or b. Data for additional N…H hydrogen bonds are presented in parentheses.

Structure	N1-N2	N2-N3	N3-N4	N1-H	N2-H	N3-H	N4-H
A1201	0.184	0.023	0.176	0.063	0.006(2×)	-	0.009
A1111	0.216	0.354	0.216	0.030	0.032	0.032	0.030
A2101	0.011	0.134	0.187	0.045 0.049	0.052	-	0.002
A2110	0.034	0.172	0.067	0.046 0.050	0.041	0.032	-
A2011	0.022	0.300	0.223	0.041(2×)	-	0.026	0.013
A2002	0.101	0.238	0.105	0.041 0.045	-	-	0.041 0.045
A3010	0.146	0.277	0.036	0.007 0.012(2×)	-	0.030	-
A3001	0.094	0.214	0.189	0.006 0.010(2×)	-	-	0.021

 doi:10.20944/preprints202407.0102.v1

B1111	0.200	0.343	0.200	0.028	0.036	0.036	0.028
B2110	0.038	0.177	0.079	0.047 0.051	0.041	0.031	-
B2101	0.016	0.149	0.182	0.039 0.043	0.057	-	0.003
B2020	0.173	0.129	0.181	0.041(2×)	-	0.007 0.022	(0.209)
B2011	0.094	0.292	0.211	0.039(2×)	-	0.031	0.019
B2002	0.095	0.241	0.102	0.040(2×)	-	-	0.040(2×)
B3010	0.130	0.272	0.028	0.005(3×)	-	0.033	-
B3001a	0.073	0.211	0.174	0.002(2×) 0.004	-	-	0.021
B3001b	0.069	0.205	0.185	0.005(3×)	-	-	0.012

Table 7. BCP ellipticity of N-N and N-H bonds in the optimized Cmnpq and Dmnpq structures. The different structures with the same notation are distinguished by additional letters a, b, c, or d. Data for additional N…H hydrogen bonds are presented in parentheses.

Structure	N1-N2	N2-N3	N3-N4	N1-N4	N1-H	N2-H	N3-H	N4-H
C1111	0.059	0.059	0.059	0.059	0.039	0.039	0.039	0.039
C2200	0.022	0.209	0.270	0.209	0.005 0.004	0.005 0.004	-	-
C2110	0.052	0.052	0.163	0.232	0.002 0.005	0.029	0.038	-
C2101	0.072	0.181	0.186	0.067	0.001 0.005	0.031	-	0.026
C2020	0.222	0.222	0.222	0.222	0.003(2×)	-	0.003(2×)	-
D(02)(20)a	0.008	-	0.008	-	(0.006)	0.030(2×)	0.030(2×)	(0.006)
D(11)(20)a	0.161	-	0.018	-	0.049 (0.022)	0.005	0.032(2×)	(0.005)
D(11)(20)b	0.161	-	0.018	-	0.005	0.004 (0.020)	0.032(2×)	(0.005)
D(22)(00)a	-	0.005	0.832	-	0.049 0.045	0.049 0.045	(0.676)	-
D(22)(00)b	0.011	-[a]	0.003	-	0.045 0.049	0.044 0.049	(0.637)	(0.621)
D(22)(00)c	0.010	-	0.003	0.653	0.049 0.045	0.049 0.045	(0.629)	-
D(22)(00)d	0.010	0.330	0.005	-	0.049 0.045	0.049 0.045	-	(0.354)
D(31)(00)a	0.151	0.316	0.003	-	0.011(2×) 0.009	0.076	(0.220)	-
D(31)(00)b	0.145	-	0.004	-	0.009 0.011(2×)	0.078	(0.266)	(1.271)

Remarks: [a] BCP ellipticity of the N1-N3 bond is 0.634.

 doi:10.20944/preprints202407.0102.v1

Similarly to [17], the charges (Table 8) on the lateral N1 and N4 atoms in the A and B structures are more negative than on the central N2 and N3 atoms. Negative N charges in the A, B and C systems (Tables 8 and 9) increase with the number of bonded H atoms. Analogously, the positive hydrogen charges increase with the number of H atoms bonded to the same nitrogen. The charges of the H atoms bonded to the central N2 and N3 atoms in the A and B systems are more positive than their lateral N1 and N4 analogs. The D systems contain practically neutral N atoms in the N_2 subsystems, and their negative charges in other subsystems increase with the number of bonded H atoms (Table 9). N…H hydrogen bonds and N…N non-bonding interactions (Table 9 and Figure S4 in Supplementary Materials) affect the N and H charges as well.

Table 8. Atomic charges of N and H (bonded to N in brackets) in the optimized Cmnpq and Dmnpq structures. The different structures with the same notation are distinguished by additional letters a or b.

Structure	N1	N2	N3	N4	H(N1)	H(N2)	H(N3)	H(N4)
A1201	-0.77	-0.42	-0.03	-0.35	0.32	0.47(2×)	-	0.44
A1111	-0.55	-0.21	-0.21	-0.55	0.37	0.51	0.51	0.37
A2110	-0.72	-0.37	-0.21	-0.19	0.42(2×)	0.42	0.44	-
A2101	-0.68	-0.35	-0.02	-0.39	0.41(2×)	0.44	-	0.41
A2011	-0.71	-0.14	-0.19	-0.45	0.41(2×)	-	0.50	0.39
A2002	-0.68	-0.07	-0.07	-0.68	0.42(2×)	-	-	0.42(2×)
A3010	-0.74	-0.33	-0.21	-0.35	0.48(2×) 0.50	-	0.38	-
A3001	-0.73	-0.24	-0.11	-0.54	0.49(3×)	-	-	0.45
B1111	-0.59	-0.28	-0.28	-0.59	0.36	0.53	0.53	0.36
B2110	-0.70	-0.37	-0.23	-0.19	0.41(2×)	0.42	0.44	-
B2101	-0.68	-0.34	-0.04	-0.42	0.40(2×)	0.46	-	0.40
B2020	-0.74	-0.19	-0.48	-0.39	0.46(2×)	-	0.53(2×)	-
B2011	-0.69	-0.09	-0.21	-0.53	0.42(2×)	-	0.51	0.38
B2002	-0.71	-0.05	-0.05	-0.071	0.43(2×)	-	-	0.43(2×)
B3010	-0.72	-0.31	-0.22	-0.41	0.47(2×) 0.500	-	0.41	-
B3001a	-0.76	-0.20	-0.09	-0.59	0.49(3×)	-	-	0.36
B3001b	-0.79	-0.19	-0.08	-0.53	0.50(3×)	-	-	0.31

Table 9. Atomic charges of N and H (bonded to N in brackets) in the optimized Cmnpq and Dmnpq structures. The different structures with the same notation are distinguished by additional letters a, b, c, or d.

Structure	N1	N2	N3	N4	H(N1)	H(N2)	H(N3)	H(N4)
C1111	-0.36	-0.36	-0.36	-0.36	0.40	0.40	0.40	0.40
C2200	-0.43	-0.43	-0.44	-0.44	0.47 0.49	0.47 0.49	-	-
C2110	-0.45	-0.33	-0.38	-0.39	0.46 0.49	0.42	0.37	-
C2101	-0.44	-0.33	-0.44	-0.37	0.50(2×)	0.37	-	0.40
C2020	-0.43	-0.35	-0.43	-0.35	0.46 0.49	-	0.46 0.49	-
D(02)(20)	-0.28	-0.52	-0.52	-0.27	-	0.46 0.42	0.46 0.42	-
D(11)(20)a	-0.36	-0.36	-0.51	-0.26	0.48	0.40	0.43(2×)	-
D(11)(20)b	-0.36	-0.36	-0.51	-0.26	0.40	0.38	0.43(2×)	-
D(22)(00)a	-0.70	-0.69	0.01	-0.02	0.38(2×)	0.38(2×)	-	-
D(22)(00)b	-0.71	-0.70	0.06	0.05	0.38(2×)	0.37	-	-

 doi:10.20944/preprints202407.0102.v1

						0.39		
D(22)(00)c	-0.71	-0.70	0.06	0.07	0.38(2×)	0.38(2×)	-	-
D(22)(00)d	-0.70	-0.71	0.01	0.03	0.38(2×)	0.38(2×)	-	-
D(31)(00)a	-0.71	-0.84	0.05	0.10	0.44(2×) 0.47	0.289	-	-
D(31)(00)b	-0.72	-0.84	-0.01	0.02	0.45(2×) 0.47	0.28	-	-

3. Methods

Geometries of various isomers of neutral N_4H_4 molecules in singlet ground spin states were optimized at the CCSD (Coupled Cluster using Single and Double substitutions from the Hartree-Fock determinant) [19] level of theory using cc-pVTZ basis sets [20]. The effects of aqueous solvenst were taken into account within the SMD (Solvation Model based on the solute electron Density) solvation model [21]. The optimized structures were tested for the absence of imaginary vibrations by vibrational analysis. Gaussian16 software (Revision B.01) [22] was used for all quantum-chemical calculations. The electron structures of the systems under study were evaluated in terms of Quantum Theory of Atoms-in-Molecules (QTAIM) [18] using the AIM2000 software (version 1.0) [23].

Bond strengths were compared according to electron densities ϱ at the bond critical points (BCP). The BCP bond ellipticities ε_{BCP} were evaluated as

$$\varepsilon_{BCP} = \lambda_1/\lambda_2 - 1 \quad (9)$$

where λ_i are the eigenvalues of the Hessian of the BCP electron density within the sequence $\lambda_1 < \lambda_2 < 0 < \lambda_3$. Atomic charges were obtained by electron density integration over atomic basins up to 0.001 e/Bohr^3. Visualization and geometry modification were performed using MOLDRAW software (Release 2.0) (https://www.moldraw.software.informer.com, accessed on 9 September 2019) [24].

4. Conclusions

Unlike our previous study of tetrazanes N_4H_6 decomposition [17], we have not found any spontaneous splitting the bonds between lateral nitrogen atoms (i.e., N1-N2 and N3-N4 fissions) in tetrazenes N_4H_4 during geometry optimization. It implies that no hydrogen rearrangements in N_4H_4 species can cause that the original ^{14}N-^{14}N-^{15}N-^{15}N backbone obtained by dimerization of either ^{15}N labelled or unlabelled HN=NH would produce $^{14}N^{15}N$ molecules. This finding might explain the observation of Cahn and Powell [8] that the randomized $^{14}N^{15}N$ composition is obtained by one-electron oxidation of ^{15}N enriched hydrazines whereas four-electron oxidizing agents produce unrandomized N_2 molecules (they supposed that all four hydrogen atoms are removed from a single hydrazine molecule). It can be expected that the formation of the diamine HN=NH intermediate is more probable by four-electron oxidation as well.

The most probable N_4H_4 split products are H_2N-NH_2 and N_2 (see Table 1 for Gibbs energies), denoted as D(22)(00), which are obtained by splitting the bond between central nitrogen atoms (i.e., N2-N3 fissions) and so only $^{15}N_2$ and $^{14}N_2$ molecules are formed. Additionally, the formation of H_3N-NH and N_2 oxidation products, denoted as D(31)(00), is preferred over structures without any N-N fissions as well (see Table 1 for Gibbs energies). The formation of H_2N=N and HN=NH oxidation products (such as D(02)(20) and D(11)(20), see Table 1) is energetically less advantageous.

Hydrogen transfers in aqueous solutions are mediated by H_2O, H_3O^+ and/or OH^- species. Similarly as in our previous study of N_4H_6 decomposition [17], the lateral N and H charges in N_4H_4 have very high charges that should support such H transfers. Nevertheless, the transfer of the third hydrogen to the lateral nitrogen from the central one without splitting the bond between both central nitrogens is energetically much less advantageous in comparison with most N_4H_4 isomers as indicated by Gibbs energies of the structures NH_3-N=NH=N, denoted as A3010 and B3010 (see Table 1).

 doi:10.20944/preprints202407.0102.v1

Unlike cyclo-N_4H_6 structures [17], their cyclo-N_4H_4 analogs are stable, without any N-N fissions. Nevertheless, their very high Gibbs energies (Table 1) indicate, that their relative abundance in aqueous solution is vanishing, so their involvement in hydrazine oxidation is highly improbable.

In agreement with our previous study [17], the QTAIM analysis confirmed that single, double and triple N-N bonds exhibit BCP electron densities of ca. 0.2, 0.5 and 0.7 e/Bohr^3, respectively, with BCP ellipticities of ca 0.0, 0.2 and 0.0, respectively. Nevertheless, hydrogen bonds can cause significant deviations from these values.

Our study deals only with some thermodynamics aspects of hydrazine oxidation in aqueous solutions. We have not deal with transition states related to hydrogen transfers and the role of water molecules/ions by these transfers. For such model calculations the individual solvent molecules/ions must be included as well. Also the differences between reaction mechanisms of two- and four-electron oxidation [8] of hydrazine are worth of study. Further theoretical and experimental studies in these fields are necessary.

Supplementary Materials: The following supporting information can be downloaded at: www.mdpi.com/xxx/s1, Figure S1: Molecular graphs of optimized N_4H_4 structures in *anti*-conformation; Figure S2. Molecular graphs of optimized N_4H_4 structures in *syn*-conformation; Figure S3. Molecular graphs of optimized cyclo-N_4H_4 structures; Figure S4. Molecular graphs of optimized N_4H_4 structures after N – N bond fission.

Author Contributions: Methodology, software, investigation, writing—original draft preparation, writing—review and editing, M.B.; supervision, project administration, funding acquisition, A.G. All authors have read and agreed to the published version of the manuscript.

Funding: The authors thank the HPC center at the Slovak University of Technology in Bratislava, which is a part of the Slovak Infrastructure of High Performance Computing (SIVVP Project No. 26230120002, funded by the European Region Development Funds), for computing facilities.

Data Availability Statement: All necessary research data are presented in the article and in Supplementary Materials.

Conflicts of Interest: The authors declare no conflicts of interest.

References

1. Davis, S. M.; Yilmaz, N. Advances in Hypergolic Propellants: Ignition, Hydrazine, and Hydrogen Peroxide Research. Adv. Aerospace Eng. 2014, 729313.
2. Lauko, L.; Hudec, R.; Lenghartova, K.; Manova, A.; Cacho, F.; Beinrohr, E. Simple Electrochemical Determination of Hydrazine in Water. Pol. J. Environ. Stud. 2015, 24(4), 1659-1666
3. Nguyen, H. V. N.; Chenoweth, J. A.; Bebarta, V. S.; Albertson, T. E.; Nowadly, C. D. The Toxicity, Pathophysiology, and Treatment of Acute Hydrazine Propellant Exposure: A Systematic Review. *Military Med. 2021,* 186, e319–e326.
4. Gutbier, A.; Neudlinger, K. Katalyse des Hydrazins durch Platinmohr. Z. Phys. Chem. 1913, 84A, 203-249.
5. Heitbaum, J.; Vielstich, W. Untersuchungen zur Ammoniakbildung bei der Hydrazinzersetzung, Electrochim. Acta 1972, 17, 1529-1542.
6. Petek, M.; Bruckenstein, S. An Isotopic Labeling Investigation of the Mechanism of the Electrooxidation of Hydrazine at Platinum. An Electrochemical Mass Spectrometric Study. Electroanal. Chem. Interrac. Electrochem. 1973, 47, 329-333.
7. Higginson, W. C. E.; Sutton, D. The Oxidation of Hydrazine in Aqueous Solution. Part II. The Use of ^{15}N as a Tracer in the Oxidation of Hydrazine. J. Chem. Soc. 1953, 1402 -1406.
8. Cahn, J. W.; Powell, R. E. Oxidation of Hydrazine in Solution. J. Am. Chem. Soc, 1954, 76, 2568-2572
9. Karp, S.; Meites, L. The Voltammetric Characteristics and Mechanism of Electrooxidation of Hydrazine, J. Am. Chem. Soc. 1962, 84, 906 – 912.
10. Wiberg, N.; Bachhuber, H.; Fischer, G. Isolation of Pure Diimine. Angew. Chem. Int. Ed. 1972, 11, 829-830.
11. Wiberg, N.; Bayer, H.; Bachhuber, H. Isolation of Tetrazene, N_4H_4. Angew. Chem. Int. Ed. 1975, 14, 177 – 178.

 doi:10.20944/preprints202407.0102.v1

12. Veith, M.; Schlemmer, G. Die Kristall- und Molekulstruktur von trans-Tetrazen-2 (N_4H_4) bei -90°C. Z. anorg. allg. Chem. 1982, 494, 7-19.
13. Zhao, M.; Gimarc, B. M. Strain Energies of (NH), Rings, n = 3-8. J. Phys. Chem. 1994, 98, 7497-7503.
14. Ball, D. W. High-level ab initio calculations on hydrogen– nitrogen compounds. Thermochemistry of tetrazetidine, N_4H_4. J. Mol. Struct. (Theochem) 2002, 619, 37–43.
15. Feng, Y.; Zhu, H.; Zhang, Q.; Zhao, Q.; Zhao, H.; Suo, B.; Zhai, G.; Zou, W.; Han, H.; Song, Q.; Li, J.; Li, Y. Theoretical study on the two novel planar-type all-nitrogen N_4^{4-} anions: Structures, stability, reaction rate and their stable mechanisms via protonation. Chem. Phys. Let. 2021, 771, 138519.
16. Hu, A.; Zhang, F. A hydronitrogen solid: high pressure ab initio evolutionary structure searches. J. Phys. Cond. Mat. 2011, 23, 022203.
17. Breza, M.; Manova, A. Hydrazine Oxidation in Aqueous Solutions I: N4H6 Decomposition. Inorganics 2023, 11, 413.
18. Bader, R.F.W. Atoms in Molecules: A Quantum Theory; Clarendon Press: Oxford, UK, 1990; ISBN 9780198558651.
19. Scuseria, G.E.; Janssen, C.L.; Schaefer, H.F., III. An efficient reformulation of the closed-shell coupled cluster single and double excitation (CCSD) equations. J. Chem. Phys. 1988, 89, 7382–7387.
20. Dunning, T.H., Jr. Gaussian basis sets for use in correlated molecular calculations. I. The atoms boron through neon and hydrogen. J. Chem. Phys. 1989, 90, 1007–1023.
21. Marenich, A.V.; Cramer, C.J.; Truhlar, D.G. Universal solvation model based on solute electron density and a continuum model of the solvent defined by the bulk dielectric constant and atomic surface tensions. J. Phys. Chem. B 2009, 113, 6378–6396.
22. Frisch, G.W.; Trucks, M.J.; Schlegel, H.B.; Scuseria, G.E.; Robb, M.A.; Cheeseman, J.R.; Scalmani, G.; Barone, V.; Petersson, G.A.; Nakatsuji, H.; et al. Gaussian 16, Revision B.01; Gaussian, Inc.: Wallingford, CT, USA, 2016.
23. Biegler-König, F.; Schönbohm, J.; Bayles, D. AIM2000—A Program to Analyze and Visualize Atoms in Molecules. J. Comput. Chem. 2001, 22, 545–559.
24. Ugliengo, P. MOLDRAW: A Program to Display and Manipulate Molecular and Crystal Structures, University Torino, Torino. 2012. Available online: https://www.moldraw.software.informer.com (accessed on 9 September 2019)